JOURNAL OF SOLID STATE CHEMISTRY 71, 77–86 (1987)

Synthesis, ESR Investigation, and Optical Properties of the Potential Vibronic Laser Material $LaMgAl_{11-x}Cr_xO_{19}$

B. VIANA, A. M. LEJUS, AND D. VIVIEN

Laboratoire de Chimie appliquée de l'Etat solide, L.A. N° 302 CNRS E.N.S.C.P., 11 rue Pierre et Marie Curie, 75231 Paris Cédex 05, France

AND V. PONÇON* AND G. BOULON

Université Claude Bernard, Lyon I, Unité associée au CNRS N° 442, Physico-Chimie des Matériaux Luminescents, 69622 Villeurbanne, France

Received November 10, 1986; in revised form January 15, 1987

Cr^{3+} doped $LaMgAl_{11}O_{19}$ single crystals have been grown. The ESR spectra and the optical properties of this matrix with magnetoplumbite structure have been studied. Three kinds of isolated sites have been identified by the $^2E \rightarrow {}^4A_2$ transition associated with the Cr^{3+} ion doped into the $4f$ antiprism site, the regular $2a$ octahedral site, and the $12k$ octahedral site. Additional lines in ESR and fluorescence spectra arise from the occurrence of $4f$–$4f$ pairs even for low doping levels. The presence of the $^4T_2 \rightarrow {}^4A_2$ broad band of fluorescence makes this material a possible candidate for a red or near-infrared emitting vibronic laser.

I. Introduction

The study of lanthanide hexaaluminates $LnMAl_{11}O_{19}$ with magnetoplumbite-like structure has been undertaken in these laboratories for several years. The purpose of these investigations is to relate the structure and chemical composition of these materials with their physical properties, particularly the optical ones. A whole series of compounds $LnMgAl_{11}O_{19}$ (Ln = La, Ce, Pr, Nd, Sm, Eu, Gd) and $LaMAl_{11}O_{19}$ (M = Mg, Mn, Fe, Co, Ni) has been prepared in the form of large single crystals and their characteristics have been investigated (*1–3*). Among these materials, lanthanum hexaaluminate $LaMgAl_{11}O_{19}$ appears to be an important crystalline laser host matrix which can be doped with different ions (La^{3+} being replaceable by other lanthanide ions (*2*), Mg^{2+} by divalent transition ions (*3*), and Al^{3+}, for instance, by Cr^{3+}). Doped with Nd^{3+}, it forms the "LNA" ($La_{1-x}Nd_xMgAl_{11}O_{19}$), a high standard performance IR laser material (*4*) which gives stimulated emission at 1.054 and 1.082 μm (*5*) and may be a substitute for the YAG:Nd. Doped with Ni^{2+} ($LaMg_{1-x}Ni_xAl_{11}O_{19}$), it is a potential vibronic la-

* Saint-Gobain Recherche.

0022-4596/87 $3.00

ser material (*6*) which could lead to a tunable laser emission around 1.1 μm (*7*).

The present paper deals with the optical properties of $LaMgAl_{11}O_{19}$ doped with Cr^{3+} ions ($LaMgAl_{11-x}Cr_xO_{19}$), a compound that may be considered as a new potential Cr^{3+} vibronic laser (*8*) that may compete with the present leader alexandrite $BeAl_2O_4:Cr^{3+}$. Furthermore, in different solid-state laser materials such as gallium scandium gadolinium garnet (GSGG) (*9*, *10*), improvement of the Nd^{3+} laser efficiency is achieved by using Cr^{3+} ions as sensitizers. In LNA too, Cr^{3+} could act as a sensitizer by transferring excitation to Nd^{3+} activator ions with an increase of the laser efficiency. We report here the synthesis and the ESR and optical investigations of Cr^{3+} ions in $LaMgAl_{11-x}Cr_xO_{19}$. Laser characteristics of this material as well as chromium–neodynium energy transfer, which are under investigation in our laboratories, will be reported in further papers.

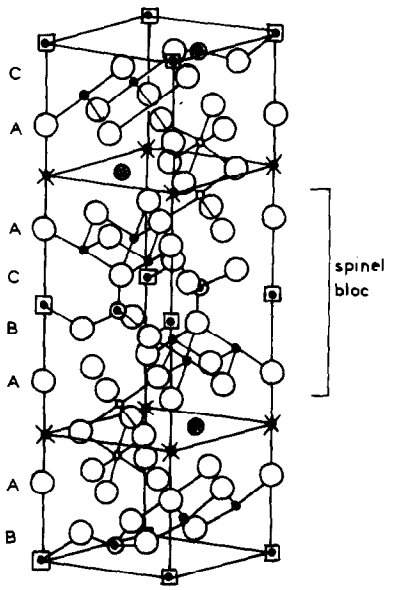

FIG. 1. The magnetoplumbite unit cell of $LaMgAl_{11}O_{19}$. (○) O^{2-}; (●) Ln^{3+}; (✕) Al^{3+}, Mg^{2+}: See Table I for identification of other symbols.

TABLE I

SOME CHARACTERISTICS OF THE DIFFERENT CATIONIC SITES AVAILABLE FOR Al^{3+} OR Mg^{2+} IN THE M.P. STRUCTURE

		Wyckoff position	Site symmetry	Mean Al–O distance	Coordinance
⊡	Regular octahedron	2*a*	D_{3d}	1.88	6
✕	Trigonal bipyramid	2*b*	C_{3v}	1.93	5
⊙	Tetrahedron	4*f*	C_{3v}	1.85	4
•	Distorted octahedron	12*k*	C_s	1.90	6
○	Antiprism	4*f*	C_{3v}	1.92	6

Note. Symbols correspond to those in Fig. 1.

II. Elaboration and Characterization of $LaMgAl_{11-x}Cr_xO_{19}$ Crystals

1. Crystal Structure of $LnMAl_{11}O_{19}$ Hexaaluminates

The magnetoplumbite-like structure (M.P.) of $LnMAl_{11}O_{19}$ hexaaluminates is hexagonal with space group $P6_3/mmc$. The unit cell (Fig. 1) is built of spinel-like blocks containing Al^{3+} and M^{2+} cations separated by mirror planes containing Al^{3+} and Ln^{3+} cations (*1*, *11*); the Wyckoff position of cations, their coordination polyhedron, and the average oxygen–cation distance are gathered in Table I.

2. Crystal Growth

In the following studies, single crystals have been grown using the Verneuil flame fusion process (*2*, *3*). In this method, a single crystal seed is fed by a powder which passes through the flame of an oxygen–hydrogen torch. The starting material is an intimate mixture of the powdered constitutive oxides (La_2O_3 5N, Rhône Poulenc, France; MgO Purity R.P., Prolabo; Al_2O_3, γ-form from Industrie des Pierres Scientifiques Djevahirdjian, Monthey, Switzerland; Cr_2O_3 Specpure, Johnson–Matthey). Rather large rod-shaped crystalline boules are obtained by this method. The various phases existing in the samples are identified by X-ray powder diffraction.

TABLE II

VARIATION OF a AND c PARAMETERS OF $LaMgAl_{11-x}Cr_xO_{19}$ ACCORDING TO x VALUES OF THE STARTING COMPOSITION

x:	0.001	.11	1	2	5.5
a (Å)	5.59_0	5.59_1	5.60_6	5.62_0	5.69_5
c (Å)	21.99_0	22.00_0	22.01_0	22.05_0	22.18_0
Phases obtained	M.P.	M.P.	M.P.	M.P. + P	

Note. M.P. = magnetoplumbite-like phase; P = perovskite phase $LaAl_{1-y}Cr_yO_3$.

3. Solubility of Chromium in $LaMgAl_{11}O_{19}$

Several compositions have been studied (*12*) according to different values of x in the formula $LaMgAl_{11-x}Cr_xO_{19}$:

—For $x \leq 1$: samples contain some large, purple single crystals (10×10 mm^2) of pure magnetoplumbite phase.

—For $1 \leq x \leq 5.5$: the Verneuil boules are polycrystalline samples containing perovskite phase ($LaAl_{1-y}Cr_yO_3$) and M.P. phase, of which some single crystalline wafers (1×1 mm^2) can be extracted.

—For $x > 5.5$: the samples are polycrystalline blocks containing the perovskite, spinel $MgCr_2O_4$, and Cr_2O_3. There is no trace of M.P. phase.

The crystal quality decreases when x increases. Simultaneously the melting point of the M.P. phase increases. This observation is probably related to the difference in melting temperature T_F of the constitutive oxides (T_F $Al_2O_3 \approx 2050$°C, T_F $Cr_2O_3 \approx 2435$°C).

The concentration dependence of the a and c parameters is shown in Table II. These variations indicate that the solubility of Cr^{3+} with respect to Al^{3+} in this structure is higher than 10% ($x = 1$) because a and c parameters continue to increase when the chromium content increases. However, for $x > 1$ there is either decomposition of M.P. phase upon cooling or noncongruent melting.

For the following studies concerning optical properties and ESR analysis, only weakly doped samples ($x \leq 0.11$) will be considered. Under these conditions large single crystals with a good crystallinity are easily prepared.

The crystals have been analyzed using an electron microprobe. It reveals, for instance, that the "pure" $LaMgAl_{11}O_{19}$ host already contains approximately 0.7×10^{20} Cr^{3+} ions cm^{-3}, chromium being a "natural" impurity of alumina. In the following studies the chromium concentrations quoted for the samples will be those coming from the analysis and not the amount added.

III. Spectroscopic Studies

1. ESR Study of Chromium-Doped Crystals

ESR experiments in the 120–300 K temperature range were carried out using a Bruker ESR 220 D X-band spectrometer, fitted with a Bruker variable-temperature accessory. Figure 2 shows the ESR spectra at 120 K of chromium-doped lanthanum hexaaluminate crystal ($[Cr^{3+}] = 2.3 \times 10^{20}$ Cr^{3+} ions cm^{-3}), the magnetic field B_0 being parallel to the c axis. The spectrum consists of a single line at $B = 338$ mT flanked by two weak satellites on its wings (Fig. 2). In the a,b plane, the spectrum is independent of the direction of the magnetic field, while the angular variation of the spectrum when B_0 rotates from c toward the a,b plane is depicted in Fig. 3. This indicates that Cr^{3+} ions are located in an axial site whose axis is the c direction of the crystal. When the chromium content increases, there is a broadening of the central ESR line (Fig. 4) because of dipolar interactions between chromium ions.

Apart from some weak lines in the 128-mT region (Fig. 2) which could be assigned to Cr^{3+} forbidden transitions ($\Delta M_s = 2$) or

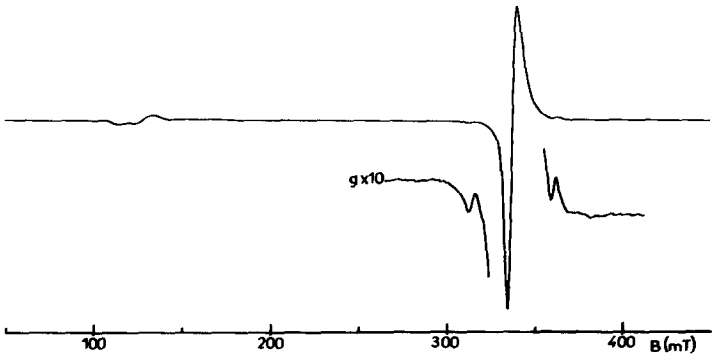

FIG. 2. X-band ESR spectrum at 120 K of a single crystalline sample with c axis parallel to B_0. $[Cr^{3+}] = 2.3 \times 10^{20}$ ions cm^{-3}; microwave frequency 9361 MHz.

trivalent iron impurities, there are no other ESR lines up to 900 mT when the magnetic field is along c. This indicates that the zero field splitting of the chromium ions in this site is large. Diagonalization of the spin Hamiltonian of the Cr^{3+} ions allows us to deduce the value of the axial zero field parameter. From the portion of the ESR line for $B_0//c$, one calculates $g_{//} = 1.977$ and assuming $g_\perp = g_{//}$ the position of the perpendicular line (*13*) gives $D = 0.97\ cm^{-1}$. From these results one can propose a localization for these Cr^{3+} ions, recalling that the large crystal field stabilization of Cr^{3+} in octahedral symmetry precludes its localization in one of the two tetrahedral sites of the M.P. unit cell (Table I). Among the three sixfold-coordinated Al/Mg sites (Table I and Fig. 1), the 12*k* and 2*a* octahedral sites must be discarded because the former ones are non-axial and the latter ones too regular to be accountable for the high Cr^{3+} D value. The remaining possibility for the site is the 4*f* antiprism close to the mirror

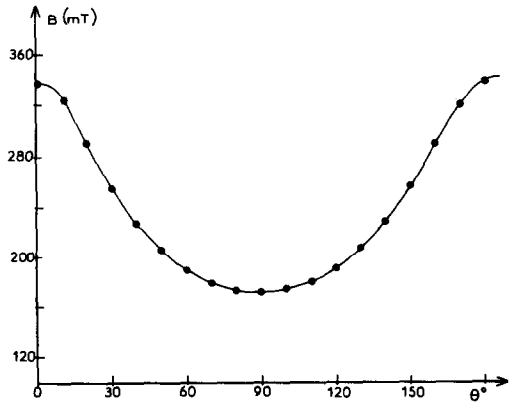

FIG. 3. Angular variation of the main line of the ESR spectrum when B_0 rotates from the c direction ($\theta = 0°$) to the (a,b) plane ($\theta = 90°$).

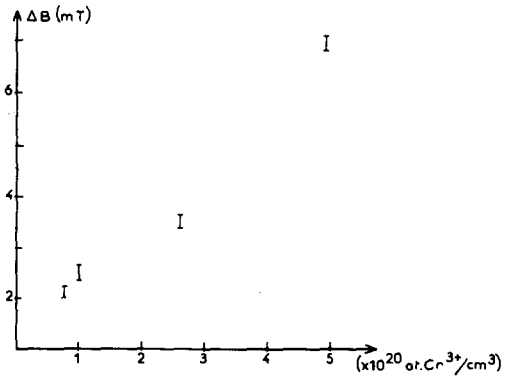

FIG. 4. Variation of the peak to peak linewidth of the central line of the ESR spectrum ($B_0//c$) according to the chromium content of the crystal.

planes (Fig. 1) with C_{3v} symmetry, the threefold axis being along c. Further remarks support this attribution:

—The antiprism site presents the largest mean Al–O distance of the unit cell. Because of the relative radius of Al^{3+} and Cr^{3+} ions, 0.67 and 0.75 Å, respectively, size effects favor chromium localization in this site. Moreover, in the isostructural compound $LaMgGa_{11-x}In_xO_{19}$, crystal structure determination (*14*) indicates that the large In^{3+} cations which substitute for Ga^{3+} ions are preferentially localized in the $4f$ antiprism.

—In the structure there are two $4f$ sites by formula unit, whose complete substitution by Cr^{3+} corresponds to $x = 2$, a value in reasonable agreement with the upper one to obtain a pure M.P. phase (cf. Section II.3).

Besides the main ESR line, few crystals also exhibit a broad and weaker line ($\Delta B \approx$ 35 mT) in their ESR spectra when B_0 rotates in the (a,b) plane. This line is slightly anisotropic, moving from 278 to 310 mT with 120° periodicity. One striking feature of this line is that it is completely missing for a rotation of B_0 in a plane containing the c axis, indicating that its intensity is strongly related to the orientation of the oscillating magnetic field B_1 of the microwave radiation with respect to the crystal axis. At the present level of investigation, one can suggest that this line arises from chromium ions with orthorhombic symmetry, and large λ value, λ being the ratio of the rhombic and axial zero field parameters. This could be the situation of Cr^{3+} in $12k$ (C_s symmetry) octahedra (Fig. 1) whose mean Al–O distance is just a little bit smaller than that of the $4f$ antiprism. Moreover, in the related compound sodium β-alumina, whose structure also contains spinel blocks presenting $2a$ and $12k$ octahedral sites (Fig. 1) but no $4f$ antiprism like in M.P.'s, optical studies have shown that Cr^{3+} ions occupy mainly these $12k$ sites.

Figure 2 shows the existence of two small satellites flanking the central ESR line which increase with chromium concentration. This could indicate that these satellites arise from Cr^{3+}–Cr^{3+} pairs. Owing to the fact that the intensity of these satellites is at its maximum for $B_0//c$, the pairs should have their internuclear axis parallel to c. This is exactly the situation corresponding to Cr^{3+} in two neighboring $4f$ antiprism sites which are close enough (2.75 Å) to develop interactions between each other.

2. Optical Properties

a. Chromium Absorption Spectrum

The room-temperature absorption spectrum of a sample of $LaMgAl_{11}O_{19}$ is given in Fig. 5. At 295 K, oscillator strengths of the $^4A_2 \rightarrow {}^4T_2$ and $^4A_2 \rightarrow {}^4T_1$ transitions are given by

$$f = \frac{1.60 \times 10^{13}}{N} \frac{n}{(n^2 + 2)^2} k_{\max} H,$$

in which n is the refractive index of the material, H the bandwidth at half-height, N the number of active chromium ions per cm^3, and $k_{\max}$ the absorption coefficient at the maximum of the line. The value of the refractive index being taken equal to 1.82, the oscillator strengths for $LaMgAl_{10.93}Cr_{0.07}O_{19}$ are $f(^4T_2) = 4.8 \times 10^{-5}$ and $f(^4T_1) = 1.8 \times 10^{-4}$.

A first evaluation of the ligand field strength can be made by the position of the maximum associated with the $^4A_2 \rightarrow {}^4T_2$ broadband which gives the D_q parameter by $D_q \approx \frac{1}{10} \times (^4A_2 \rightarrow {}^4T_2)$ in wavenumbers as can be seen in Table III. The D_q parameter for hexaaluminate is lower than that for ruby or spinels but higher than that for garnet, which is a good tunable solid-state laser. The value is practically identical to that of alexandrite, so we may assume an

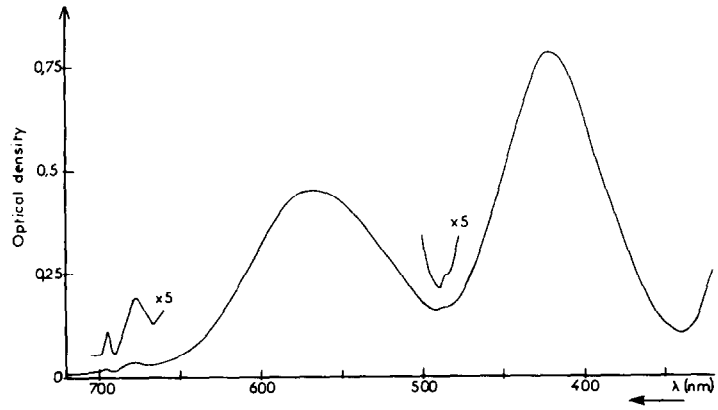

FIG. 5. Optical absorption spectrum of $LaMgAl_{11}O_{19}$: Cr (concentration 4×10^{20} Cr^{3+} ions cm^{-3}); the light propagation in the c direction of the crystal.

intermediate crystal field for the main Cr^{3+} site, yielding the possibility of observing the fluorescent transitions from both ^2E and $^4T_2$ levels (*16*).

b. Chromium Fluorescence Spectrum

All the measurements—fluorescence spectrum, lifetime decay—have been performed by exciting the sample at 532 nm with a frequency-doubled YAG : Nd^{3+} laser (width 0.1 cm^{-1}, τ = 15 nsec, frequency 10 Hz) (*15*). Two samples containing 10^{20} Cr^{3+} ions cm^{-3} and 4×10^{20} Cr^{3+} ions cm^{-3} were analyzed at room temperature and at 4.4 K. The emission spectra are shown in Fig. 7. They consist of one main peak at 695 nm due to the $^2E \rightarrow {}^4A_2$ transition with some satellite lines at 688.6 nm and a shoulder at 691 nm on the foot of the main line on the short-wavelength side and at 700.7, 707, 709, and 725 nm on the long-wavelength side. Besides, the fluorescence spectrum presents a broad band extending out to 880 nm due to $^4T_2 \rightarrow {}^4A_2$ transition, which in fact appears smaller in Fig. 6 than it is because of the bad PM response at the long wavelengths. Once again the emission spectrum profile resembles that of alexandrite crystal (*17*).

When the temperature decreases from 295 to 4.4 K, the resolution of the satellite lines increases (Figs. 8 and 9) and the width of the main line decreases from 4.0 to 3.2 nm. We clearly observe three kinds of $^2E \rightarrow {}^4A_2$ lines corresponding to three kinds of sites. This behavior arises from a great inhomogeneity in the distribution of Cr^{3+} in the structure. The main line arises from Cr^{3+} in the $4f$ while the weak lines at 691 and 688.6 nm may be connected with $12k$ and $2a$ sites. The origin of the line at 688.6 nm present at every concentration and temperature could be attributed to Cr^{3+} ions occupying $2a$ sites, as will be discussed according to its fluorescence decay time in the following section. Thus the other line at 691 nm probably corresponds to Cr^{3+}-ion-doped $12k$ sites. On the other hand, the

TABLE III

AVERAGE VALUE OF THE D_q PARAMETER IN Cr^{3+}-DOPED CRYSTALS ESTIMATED BY THE MAXIMUM OF THE $^4A_2 \rightarrow {}^4T_2$ ABSORPTION BAND AND NOT BY THE ZERO-PHONON LINE UNRESOLVED IN THE SPECTRUM

Host	Structure	D_q (cm^{-1})
$ZnAl_2O_4$	Spinel	1850
Al_2O_3 (ruby)	Corundum	1830
$MgAl_2O_4$	Spinel	1800
$LaMgAl_{11}O_{19}$ (hexaaluminate)	Magnetoplumbite	1770
$BeAl_2O_4$ (alexandrite)	Chrysoberyl	1725
$Gd_3Sc_2Ga_5O_{12}$ (GSGG)	Garnet	1590

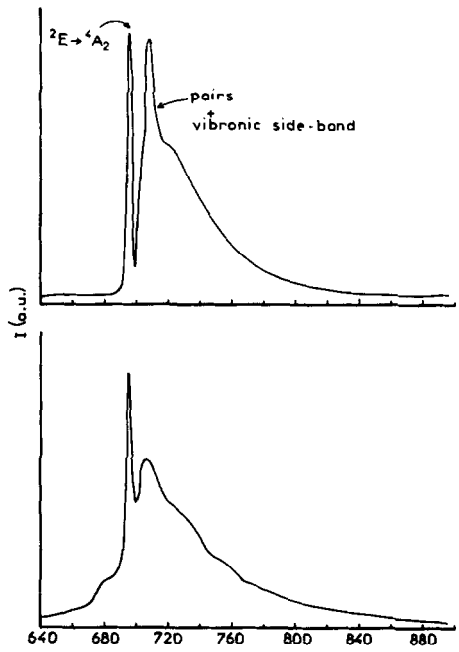

FIG. 6. Complete fluorescence spectrum at 4.4 K (above) and room temperature (below) of 4×10^{20} Cr^{3+} ions cm^{-3} in $LaMgAl_{11}O_{19}$. Excitation in the $^4T_2$ level of Cr^{3+} under λ = 532-nm laser excitation.

multisite character and the splitting of the ^2E level, because of the noncubic symmetry of the sites, could explain the broadening of this $^2E \rightarrow {}^4A_2$ line in $LaMgAl_{11}O_{19}$ compared to in other crystalline matrices. The occurrence of the $^2E \rightarrow {}^4A_2$ line indicates according to the d^3 Tanabe–Sugano diagram that the crystal field experienced by the Cr^{3+} ions giving rise to the 688.6-nm line is rather strong. However, one also observes the $^4T_2 \rightarrow {}^4A_2$ broadband emission responsible for the long tail of the fluorescence spectrum toward the long wavelengths, indicating that the crystal field is weaker than in ruby, for instance. It should be remembered that in the intermediate case of the ligand field strength, a Cr^{3+} ion gives rise to both $^2E \rightarrow {}^4A_2$ and $^4T_2 \rightarrow {}^4A_2$ transitions as it probably occurs in the $4f$ and $12k$ sites of this material.

Increasing the chromium concentration leads to an increase of the satellite lines around 710 nm (Fig. 7). It follows that the satellite peaks are probably due to Cr^{3+} pairs, as usual in the chromium-doped crystals. These fluorescence lines also overlap the vibronic spectrum of the zero phonon line for the $^2E \rightarrow {}^4A_2$ transition of chromium in the three octahedral sites.

The previous assignment is essentially consistent with (i) the presence of three octahedral sites as indicated in Table I, (ii) the population of each available kind of site in the lattice, and (iii) by the usual decreasing dependence of the $^2E \rightarrow {}^4A_2$ transition energy with the increasing of the bond length between Al^{3+} (or Cr^{3+}) and O^{2-} ions. Table I clearly shows that the mean distance increases with the $2a$, $12k$, and $4f$ site series.

c. *Chromium Fluorescence Decay*

The chromium fluorescence decay in $LaMgAl_{11}O_{19}:Cr^{3+}$ at two concentrations (10^{20} and 4×10^{20} Cr^{3+} ions cm^{-3}) has been recorded with a time scale corresponding to the $^2E \rightarrow {}^4A_2$ transition (larger than a millisecond). The fluorescence decays are expo-

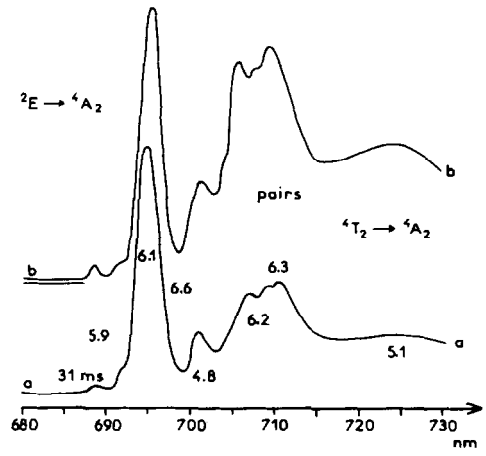

FIG. 7. Detail of the fluorescence spectra of $LaMgAl_{11}O_{19}$ under λ = 532-nm laser excitation at 4.4 K for (a) $x = 10^{20}$ Cr^{3+} ions cm^{-3} and (b) $x = 4 \times 10^{20}$ Cr^{3+} ions cm^{-3}.

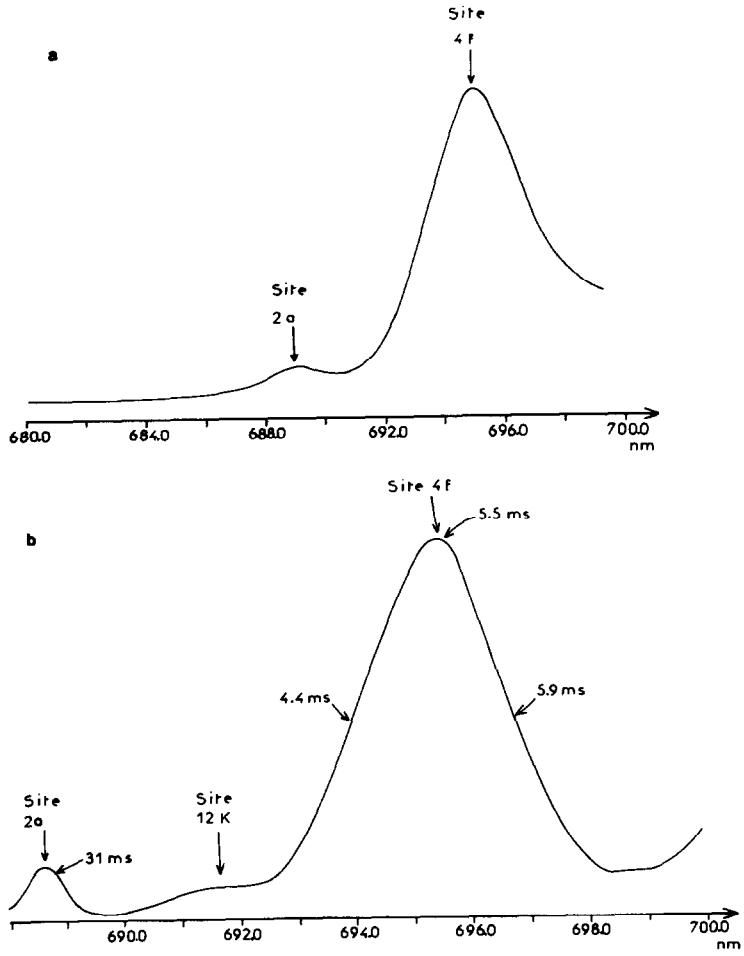

FIG. 8. High-resolution fluorescence spectra of the $^2E \rightarrow {}^4A_2$ transition of 4×10^{20} Cr^{3+} ions cm^{-3} in $LaMgAl_{11}O_{19}$ under λ = 532-nm excitation at (a) room temperature and (b) 4.4 K.

nential at 4.4 K for low Cr^{3+} concentration (Fig. 9) but not when the concentration increases. That is due to the existence of energy transfer between the $4f$ octahedral sites of the M.P. structure. The nonexponential fluorescence decay curves at room temperature (Fig. 10) indicate that phonon-assisted energy transfer occurs. The average time constant of the ^2E level (transition $^2E \rightarrow {}^4A_2$) around 695 nm varies between τ = 6.13 msec at low chromium concentration and τ = 5.47 msec for a chromium concentration of 4×10^{20} Cr^{3+} ions cm^{-3}. These variations and the nonexponential decay reveal energy transfer between the $^2E \rightarrow {}^4A_2$ and $^4T_2 \rightarrow {}^4A_2$ overlapping bands or within the $4f$ antiprism sites themselves and also between the $4f$ sites and the $4f$ strongly perturbed sites of the chromium pairs. The value of the time constant for the weak line (688.6 nm) is very high, approximately τ = 31 msec; this indicates that the transition corresponds to a very symmetric octahedral site, as for the $2a$ sites of the M.P. structure. The relatively weak intensity of this fluorescence line indicates a very low population of the $2a$ sites in good agreement with the crystal-

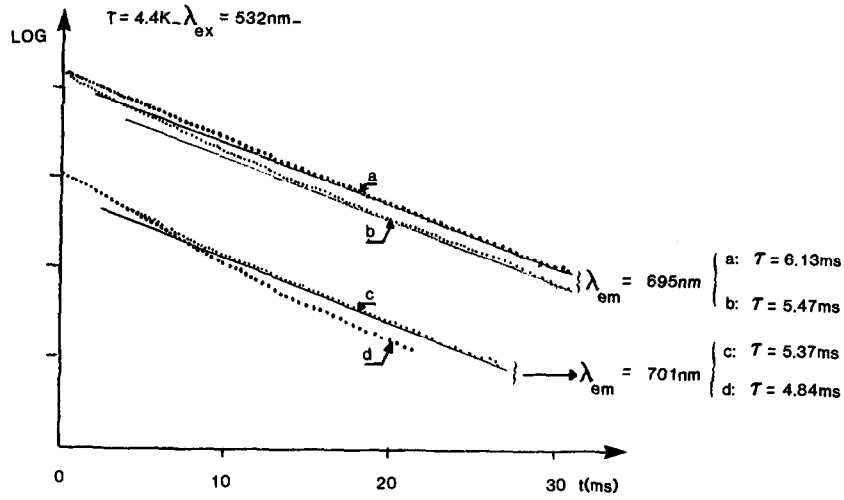

FIG. 9. 4.4 K fluorescence decay of Cr^{3+} $LaMgAl_{11}O_{19}$ at two particular emission wavelengths λ_{em} (see Fig. 7). (a, d) 10^{20} Cr^{3+} ions cm^{-3}; (b, c) 4×10^{20} Cr^{3+} ions cm^{-3}; $\lambda_{excit} = 532$ nm. The values indicate the time constant of the long part of the decay.

lographic data. A similar interpretation has been proposed in β-alumina: Cr^{3+} for a fluorescence line with $\tau = 50$ msec (*18*).

The slopes of the semilog curves at 4.4 K are almost identical at long times as can be seen in Fig. 9 for both octahedral regular sites and perturbed sites as well as for $^2E \rightarrow {}^4A_2$ transitions and for $^4T_2 \rightarrow {}^4A_2$ broadband emission. It means there is either a thermal equilibrium between $^4T_2$ and ^2E excited levels or energy transfer between each type of site which is governed by the long-lived ^2E level.

The two hypotheses are likely but the latter one has our preference because we observe a slight deviation from exponential

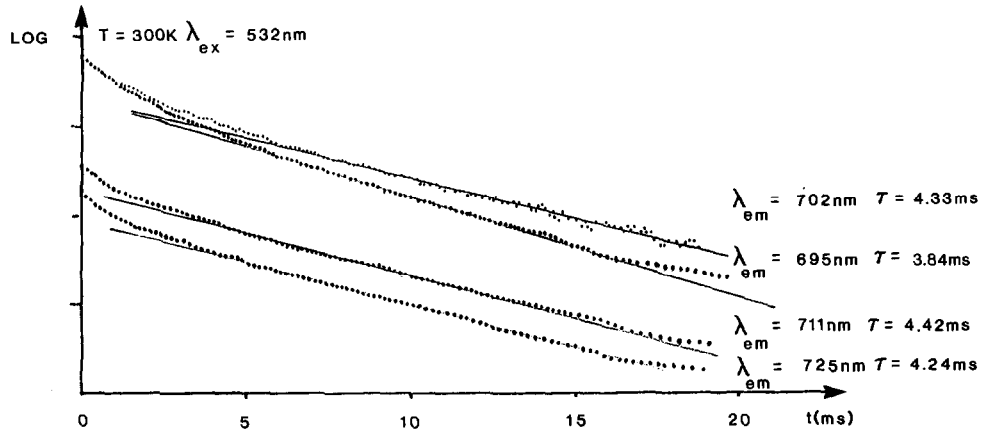

FIG. 10. Room-temperature fluorescence decay of Cr^{3+} in $LaMgAl_{11}O_{19}$ for several emission wavelengths λ_{em}, under $\lambda = 532$-nm excitation (chromium content 4×10^{20} ions cm^{-3}).

behavior at very short times at 4.4 K and a stronger deviation at room temperature. Moreover, it seems that energy transfer occurs not only from the main $4f$ sites but also from $2a$ sites because a long tail may be detected in the long time portion with a very weak intensity. Such a time dependence has also been seen with other Cr^{3+}-doped materials and seems to be a characteristic of the Cr^{3+} activator ion (*16, 19–21*).

IV. Conclusion

The great solubility of chromium into $LaMgAl_{11}O_{19}$ matrix allows us to grow good single crystals with uniform doping and good quality. At this step of our investigations, we have identified that the $^2E \rightarrow {}^4A_2$ transition of Cr^{3+} ions enters mainly into the $4f$ antiprism of the M.P. structure but also into the regular $2a$ octahedral sites and in the $12k$ octahedral sites. Additional lines in ESR and fluorescence spectra arise from the occurrence of $(4f)Cr$–$(4f)Cr$ pairs even for low doping levels. The presence also of the $^4T_2 \rightarrow {}^4A_2$ broadband luminescence extending toward the long wavelengths in $LaMgAl_{11-x}Cr_xO_{19}$ makes this material a possible candidate for a red or near-infrared emitting vibronic laser. However, there are still a number of parameters to study such as crystal quality, optimal chromium concentration, laser emission cross sections, excited state absorption, and so on. These studies are now in progress; further work in this study will be to consider the energy transfer between Cr^{3+} and Nd^{3+} in $LaMgAl_{11}O_{19}$:Nd,Cr in order to improve the laser emission efficiency of LNA.

Acknowledgment

The authors thank Dr. F. Laville for the determination of the chromium solubility in $LaMgAl_{11}O_{19}$.

References

1. A. Kahn, A. M. Lejus, M. Madsac, J. Thery, D. Vivien, and J. C. Bernier, *J. Appl. Phys.* **52**(11), 6864 (1981).
2. D. Saber and A. M. Lejus, *Mater. Res. Bull.* **16**(10), 1325 (1981).
3. F. Laville and A. M. Lejus, *J. Cryst. Growth* **63**, 426 (1983).
4. D. Vivien, A. M. Lejus, J. Thery, R. Collongues, J. J. Aubert, R. Moncorgé, and F. Auzel, *C.R. Acad. Sci. Paris sér. II* **298**(6), 195 (1984).
5. L. D. Schearrer, M. Leduc, D. Vivien, A. M. Lejus, and J. Thery, *IEEE J. Quantum Electron.* **22**(5), 713 (1986).
6. F. Laville, M. Perrin, A. M. Lejus, M. Gasperin, R. Moncorgé, and D. Vivien, *J. Solid State Chem.*, in press.
7. R. Moncorgé, T. Benyattou, D. Vivien, and A. M. Lejus, *J. Lumin.* **35**, 199 (1986).
8. P. Hammerling, A. B. Budgor, and A. Pinto, "Tunable Solid State Lasers," Series No. 47, Springer-Verlag, New York/Berlin (1985).
9. E. V. Zharikov *et al.*, *Soviet J. Quantum Electron.* **13**, 82–85 (1983).
10. D. Pruss, G. Huber, A. Beimowski, W. Laptev, I. A. Shcherbakov, and Y. D. Zharitov, *Appl. Phys. B* **28**, 355–358 (1982).
11. M. Gasperin, M. C. Saine, A. Kahn, F. Laville, and A. M. Lejus, *J. Solid State Chem.* **54**, 61 (1984).
12. F. Laville, Thèse d'Etat, Université P. & M. Curie, Paris (1985).
13. Wertz Bolton, "Electron Spin Resonance: Elementary Theory and Practical Applications," McGraw–Hill, New York (1972).
14. D. Lefebvre, A. Kahn, and J. Thery, to be published.
15. G. Boulon, "Energy Transfer Process in Condensed Matter" (B. Di Bartolo, Ed.), ASI Series B, Physics, Vol. 114, Plenum, New York (1984).
16. G. Boulon, "Materials Chemistry and Physics," **16**, 301 (1987).
17. R. Powell, L. Xi, X. Gang, and G. Quarles, *Phys. Rev. B* **32**, 2788 (1985).
18. G. Mariotto, M. Montagna, and F. Rossi, *J. Phys. (Orsay, Fr.)* **46**, C7, 343 (1985).
19. M. Bouderbala, G. Boulon, A. Kisilev, R. Reisfeld, A. Buch, M. Ish-Shalom, and A. M. Lejus, *Chem. Phys. Lett.* **121**, 535 (1985).
20. V. Ponçon, M. Bouderbala, G. Boulon, A. M. Lejus, R. Reisfeld, A. Buch, and M. Ish-Shalom, *Chem. Phys. Lett.* **130**, 444 (1986).
21. A. Van Die, G. Blasse, and W. F. Van der Weg, *J. Phys. C* **18**, 3379 (1985).